Earth and Planetary Science Letters 583 (2022) 117444

Contents lists available at ScienceDirect

Earth and Planetary Science Letters

www.elsevier.com/locate/epsl

Frictional controls on the seismogenic zone: Insights from the Apenninic basement, Central Italy

G. Volpe [a,*], G. Pozzi [b], E. Carminati [a], M.R. Barchi [c], M.M. Scuderi [a], E. Tinti [a], L. Aldega [a], C. Marone [a,d], C. Collettini [a]

[a] Università degli Studi di Roma, La Sapienza, Italy
[b] Istituto Nazionale di Geofisica e Vulcanologia, Italy
[c] Dipartimento di Fisica e Geologia, Università degli Studi di Perugia (CRUST Member, Centro inteRUniversitario per l'analisi SismoTettonica tridimensionale con applicazioni territoriali), Italy
[d] Department of Geoscience, The Pennsylvania State University, USA

ARTICLE INFO

Article history:
Received 29 November 2021
Received in revised form 9 February 2022
Accepted 14 February 2022
Available online 1 March 2022
Editor: R. Bendick

Keywords:
earthquakes
rheology
friction
structural heterogeneities
basement
seismogenic regime

ABSTRACT

Crustal seismicity is in general confined within the seismogenic layer, which is bounded at depth by processes related to the brittle-ductile transition (BDT) and in the shallow region by fault zone consolidation state and mineralogy. In the past 10-15 years, high resolution seismological and geodetic data have shown that faulting within and around the traditional seismogenic zone occurs in a large variety of slip modes. Frictional and structural heterogeneities have been invoked to explain such differences in fault slip mode and behaviour. However, an integrated and comprehensive picture remains extremely challenging because of difficulties to properly characterize fault rocks at seismogenic depths. Thus, the central-northern Apennines provide a unique opportunity because of the integration of deep-borehole stratigraphy and seismic reflection profiles with high resolution seismological data and outcrop studies. These works show that seismic sequences are limited within the sedimentary cover (depth < 9-10 km), suggesting that the underlaying basement plays a key-role in dictating the lower boundary of the seismogenic zone.

Here we integrate structural data on exhumed outcrops of basement rocks with laboratory friction data to shed light on the mechanics of the Apenninic basement. Structural data highlight heterogeneous and pervasive deformation where foliated and phyllosilicate-rich rocks surround more competent quartz-rich lenses up to hundreds of meters in thickness. Phyllosilicate horizons deform predominantly by folding and foliation-parallel frictional sliding whereas quartz-rich lenses are characterized by brittle signatures represented by extensive fracturing and minor faulting. Laboratory experiments revealed that quartz-rich lithologies have relatively high friction, $\mu \approx 0.51$, velocity-strengthening to neutral behaviour, and elevated healing rates. On the contrary, phyllosilicate-rich (muscovite and chlorite) lithologies show low friction, $0.23 < \mu < 0.31$, a marked velocity strengthening behaviour that increases with increasing sliding velocity and negligible rates of frictional healing.

Our integrated approach suggests that in the Apenninic basement deformation occurs along shear zones distributed on thickness up-to several kilometres, where the frictionally stable, foliated, and phyllosilicate-rich horizons favour aseismic deformation and therefore confine the depth of major earthquake ruptures and the seismogenic zone.

1. Introduction

The seismogenic regime is defined by the distribution of background microearthquake activity within the upper 10-15 km of the continental crust (Sibson, 1989). The base of the seismogenic regime, or the brittle-ductile transition (hereinafter, BDT) represents a transition zone from elasto-frictional faulting along localised brittle structures to viscous shearing in thick mylonites (e.g., Sibson, 1977; Scholz, 2019). In this canonical view, the base of the BDT is mainly constrained by the extrapolation of quartzite flow laws that place the transition at about 300-350 °C (Brace and Kohlstedt, 1980; Chen and Molnar, 1983).

Frictional arguments, building on rate and state friction, have proposed that within the seismogenic layer, earthquake nucleation

* Corresponding author.
E-mail address: giuseppe.volpe@uniroma1.it (G. Volpe).

https://doi.org/10.1016/j.epsl.2022.117444

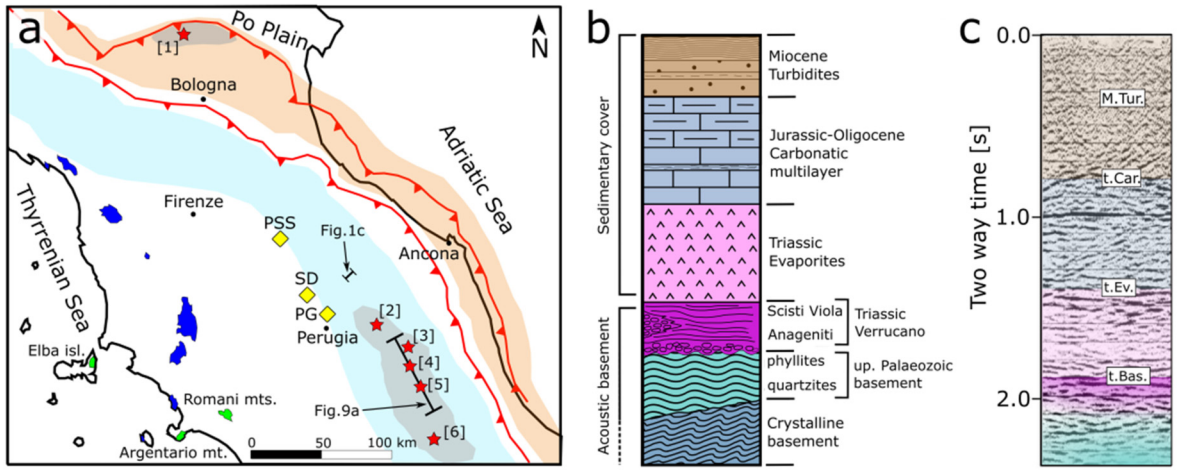

Fig. 1. a) Location map of the study area. Mainshocks (red stars: [1], Emilia 2012; [2] Colfiorito 1997; [3] Visso 2017; [4] Norcia 2017; [5] Amatrice 2017; [6] L'Aquila 2009) and aftershocks (shaded grey area) of the major seismic sequences since 1997. Yellow diamonds mark locations of deep-boreholes where acoustic basement was encountered: PSS-Pieve Santo Stefano, SD-San Donato, PG-Perugia 1. Blue and green to the west show basement outcrop locations; studied and sampled outcrops are represented in green. Black arrows indicate sections reported in Fig. 1c and Fig. 9a. Red lines represent major thrust faults. Active compressional (red shaded area) and active extensional (blue shaded area) areas constrained by GPS (Anderlini et al., 2016) and stress measurements (Montone and Mariucci, 2016). b) Stratigraphic column of the Umbria-Marche region consisting of Miocene turbidites, Jurassic-Oligocene carbonates and Triassic Evaporites laying above the "acoustic basement": Verrucano formation (Triassic) and upper Palaeozoic basement. c) Time-migrated seismic profile (location in panel a) approximatively corresponding to a 7.5 km thick stratigraphic column: M.Tur., Miocene turbidites; t.Car., top Jurassic-Oligocene carbonatic multilayer; t.Ev., top Triassic Evaporites; t.Bas., top acoustic basement (modified from Collettini and Barchi, 2002). (For interpretation of the colours in the figure(s), the reader is referred to the web version of this article.)

is promoted by the rate-weakening behaviour induced by localization along brittle faults (Dieterich, 1979; Marone and Scholz, 1988; Beeler et al., 1996; Scholz, 1998). In this framework, the seismogenic layer is confined at depth by the viscously deforming mylonites, and at shallow (1-2 km) levels by cataclastic flow at low confining pressure involving velocity strengthening and dilatancy-hardening (Scholz, 1998). However, in the last 10-15 years high-resolution seismological and geodetic data have documented a large gamut of fault slip behaviour along structures belonging to the elasto-frictional regime. For example, aseismic creep and repeating earthquakes have been documented along some segments of the San Andreas fault (Waldhauser et al., 2004) or along extensional detachments (Chiaraluce et al., 2007). Aseismic slip is sometimes prevalent over the entire depth range of the seismogenic portions of subduction megathrusts (Perfettini et al., 2010; Avouac, 2015), calling into question the simple concepts and methods used to define the seismogenic zone. Moreover, slow slip events appear to be ubiquitous on seismic faults (e.g., Jolivet and Frank, 2020) where they play an important role throughout the earthquake cycle (Bürgmann, 2018 and references therein). Finally, accelerated creep has been recorded during hydraulic stimulations of faults (Eyre et al., 2019; Cappa et al., 2019).

Several arguments have been proposed to explain the observed spectrum of fault slip behaviour. Friction laboratory experiments indicate that slow slip events arise near the threshold between stable and unstable failure and are controlled by fault frictional properties, the effective normal stress and the stiffness of the fault loading medium (e.g., Baumberger et al., 1994; Gu and Wong, 1994; Leeman et al., 2016; Scuderi et al., 2017; Mclaskey and Yamashita, 2017; Marone, 2019; Passelègue et al., 2019; Bedford and Faulkner, 2021). Works building on the integration of rheological and mechanical data indicate that structural and frictional heterogeneities are relevant for complex fault slip behaviour (e.g., Tesei et al., 2014; Collettini et al., 2019; Fagereng and Beall, 2021).

Although recent works have significantly improved our understanding of the beauty and complexity of fault slip behaviour, an integrated and comprehensive picture that incorporates structural and frictional aspects of the seismogenic zone remains unresolved. Here, we integrate subsurface geology and seismological data from the Apennines with structural observations and friction experiments on rocks that represent exhumed analogues of those present at seismogenic depths to propose a model in which the seismogenic zone, and confinement at depth of the major seismic sequences of the Apennines, is dictated by the frictional, rate-strengthening properties of basement rocks.

2. Seismicity distribution and the Apenninic basement

From the Oligocene to the present day, the central-northern Apennines have experienced two phases of eastward migrating deformation: an early compression with eastward directed thrusting and a later phase of extension (e.g., Carminati et al., 2012). Compressional tectonics is now active in the Adriatic coast and Po Plain (Carminati et al., 2012; Govoni et al., 2014; Montone and Mariucci, 2016) whereas active extension (Fig. 1a) is located along the axial zone of the Apennines (e.g., Montone and Mariucci, 2016). This seismo-tectonic setting makes the Apenninic chain one of the most seismically active area in Europe, as confirmed by four catastrophic seismic sequences since 1997: Colfiorito 1997-98, L'Aquila 2009, Emilia 2012, and Amatrice-Norcia 2016-17. In this region, 150 years of work on surface geology and stratigraphy (Centamore et al., 1986; Cresta et al., 1989), the availability of an extensive dataset of seismic reflection profiles (Bally et al., 1986; Pialli, 1998) and high-resolution seismic data (Chiaraluce et al., 2003, 2017; Improta et al., 2019; Chiarabba et al., 2009, 2014; Waldhauser et al., 2021) allow for a unique comparison between geological and seismological data. From this comparison several common aspects have been noted: a) the mainshocks ($M > 5$) of all the seismic sequences nucleate within the Triassic evaporites (Mirabella et al., 2008; Govoni et al., 2014; Baccheschi et al., 2020; Barchi et al., 2021; Buttinelli et al., 2021); b) Seismicity occurs within the sedimentary cover (Mirabella et al., 2008; Govoni et al., 2014; Barchi and Collettini, 2019; Baccheschi et al., 2020; Barchi et al., 2021), with aftershock distributions mainly confined between 1 and 10 km of depth (Chiaraluce et al., 2003, 2017; Chiarabba et al., 2009, 2014); c) the base of the sedimentary cover and its contact with the basement marks the transition from seismic to aseismic deformation (Barchi et al., 2021).

In the area of active Apenninic extension, the basement is present only at seismogenic depths. It has been drilled by few

Table 1
Summary of lithology and mineral content of the sampled basement rocks. See Fig. 1 for the location of the outcrops.

Formation	Rock	Lithology	Mineralogy	Outcrop
Verrucano formation	Scisti Viola	phyllites	Quartz = 37% Phyllosilicates = 46% Oxides = 17%	Eastern Elba Island
	Anageniti	meta-conglomerates	Quartz = 66% Phyllosilicates = 24% Carbonates = 8% Oxides = 2%	Monte Argentario
Upper Palaeozoic basement	phyllites	phyllites	Quartz = 36% Phyllosilicates = 58% Oxides = 6%	Monti Romani
	quartzites	meta-quartzarenites	Quartz = 65% Phyllosilicates = 33% Oxides = 2%	Monti Romani

deep boreholes: San Donato, Pieve Santo Stefano, and Perugia wells (Bally et al., 1986; Anelli et al., 1994; Barchi et al., 1998, and Fig. 1a). In some of these boreholes, the tectonic superposition of basement slices above the Triassic Evaporites indicates that some major thrust faults are rooted at least within the shallower portion of the basement (Barchi et al., 1998; Scrocca et al., 2005). In seismic reflection profiles the basement is characterized by a set of oblique, medium to high amplitude, low-continuity reflections, contrasting with the overlying transparent facies of the Evaporites (Fig. 1c). These peculiar seismic facies have been defined as the "acoustic basement" (Bally et al., 1986; Barchi et al., 1998; Mirabella et al., 2008). The boundary between the evaporites and the basement also corresponds to an important inversion in seismic velocity, with Triassic evaporites, characterised by Vp = 6.0 – 6.3 km/s (Bally et al., 1986; Trippetta et al., 2013) and the acoustic basement with Vp at about 5.0 km/s (Bally et al., 1986; Ponziani et al., 1995; Montone and Mariucci, 2020). Some interpretations of seismic profiles suggest a basement with a thickness up to 7.5 km (Patacca et al., 2008).

Since extensional tectonic migrated eastwardly with time from the Tyrrhenian Sea to Apenninic chain, extension in the Tyrrhenian islands and Tuscany has been active for enough time to change the geological and geophysical character of the area and to allow exhumation of basement rocks (Fig. 1a). Here we have studied the basement rocks corresponding to the "acoustic basement" in boreholes and seismic reflection profiles. This basement is represented by Triassic clastic deposits (Verrucano formation) that overlies low grade meta-sediments belonging to the foredeep-foreland system of the Hercinic chain, upper Palaeozoic basement (Bally et al., 1986; Lazzarotto et al., 2003; Carminati and Doglioni, 2012; and Fig. 1b). The Verrucano formation consists of two main lithologies: phyllites (Scisti Viola) and meta-conglomerates (Anageniti, Aldinucci et al., 2008; Cassinis et al., 2018). The upper Palaeozoic basement is represented by Carboniferous phyllites and quartzites of low metamorphic grade (Moretti et al., 1990; Verrucchi et al., 1994; Pandeli et al., 1994).

3. Materials and methods

3.1. Structural geology and rock sampling

We studied the Verrucano formation and the upper Palaeozoic basement in selected outcrops in the Tuscany region (Fig. 1a and Table 1). We focused on characterizing the lithological and structural heterogeneities of exhumed shear zones of the basement at the meso-scale (< km) together with the distribution of competent vs. incompetent lithologies. Representative endmember lithologies from each locality were chosen and analysed with the optical microscope (details in paragraph 4.2). From the Verrucano formation we sampled quartz-meta-conglomerates, Anageniti, and phyllites, Scisti Viola (Tongiorgi et al., 1977; Aldinucci et al., 2008) while for the upper Palaeozoic basement, quartzite and phyllites (Moretti et al., 1990).

3.2. X-ray diffraction (XRD) analysis

The mineralogical composition of the sampled rocks was determined by XRD analysis on the same powders used for the friction experiments (grain size, $\phi < 125$ μm). The analysis was conducted using a Bruker D8 Advance X-ray system equipped with Lynxeye XE-T silicon-strip detector at the Department of Earth Sciences, Sapienza University of Rome. The instrument was operated at 40 kV and 30 mA using CuKα radiation ($\lambda = 1.5406$ Å). Samples were run between 2–70° 2θ with step sizes of 0.02° 2θ while spinning the sample. Data were collected with variable slit mode to keep the irradiated area on the sample surface constant and converted to fixed slit mode for semiquantitative analysis. Semiquantitative estimation of mineral phases was performed by calculating peak areas and using mineral intensity factors as calibration constants (Moore and Reynolds, 1997).

3.3. Friction experiments

Friction experiments were conducted using BRAVA (Brittle Rock deformAtion Versatile Apparatus), a servo-controlled biaxial testing apparatus (Collettini et al., 2014). Experiments were performed in the Double Direct Shear configuration (DDS) consisting of three steel grooved blocks which sandwich two identical layers of gouge or intact rock wafers. Normal and shear stress are applied by fast-acting hydraulic servo-controlled rams and measured by strain gauged load-cells with an accuracy of ± 0.03 kN in a range from 0.2 kN to 1.5 MN. Stresses are obtained using the contact sample area (5 x 5 cm^2). The vertical and horizontal load point displacement are measured by LVDT (linear variable displacement transformers) with an accuracy of ± 0.1 μm (Collettini et al., 2014). The displacement time series were corrected for the elastic stretch of the load frame, considering that the machine stiffness is 329.50 kN/mm on the horizontal direction and 386.12 kN/mm on the vertical direction. Data were sampled at frequencies of 1 Hz to 1 kHz and recorded continuously with a 16 channel 24-bit analog to digital acquisition system (Collettini et al., 2014).

Two types of experimental samples were tested: one using gouge formed from for all the sampled lithologies and another using intact wafers only for foliated lithologies (phyllites and quartzites of upper Palaeozoic basement). The gouge was produced by crushing, milling, and sieving ($\phi < 125$ μm) the sampled rocks whereas the intact wafers were obtained by cutting the sampled rocks, according with their in-situ orientation, in parallelepipeds of 5 x 5 cm^2 of area and 1.0 cm of thickness.

Table 2
Experimental results for the tested lithologies. "/" symbol indicated missing data related to premature end of experiments.

Formation	Rock	Type	σn	Experiment	μss	Healing rate	*a-b*
Verrucano	Scisti Viola	gouge	25	b996	0.28	−0.00064	0.0034
			50	b997	0.28	0.00023	0.0035
			75	b998	0.29	0.00044	0.0031
			100	b999	0.29	0.00112	0.003
	Anageniti	gouge	25	b1003	0.52	0.00742	0.0008
			50	b1006	0.51	0.00674	0.0011
			75	b1008	0.51	0.00707	0.0014
			100	b1007	0.51	0.00682	0.0017
Upper Palaeozoic basement	phyllites	gouge	25	b955	0.33	0.00142	0.0007
			50	b973	0.34	0.00176	0.0022
			75	b974	0.34	0.00193	0.0025
			100	b975	0.32	0.00154	/
		wafer	10	b1009	0.27	0.00046	0.0034
			25	b981	0.19	0.00091	0.0031
			35	b1011	0.35	/	/
			50	b985	0.20	0.00036	0.0026
	quartzites	gouge	25	b987	0.49	0.00474	0.0022
			50	b988	0.49	0.00471	0.0019
			75	b989	0.48	0.00468	0.0021
			100	b990	0.48	0.00485	0.0023
		wafer	10	b1004	0.32	/	/
			25	b995	0.24	0.00149	0.0024
			35	b1002	0.25	0.00138	0.0026
			50	b991	0.27	0.00129	0.0025

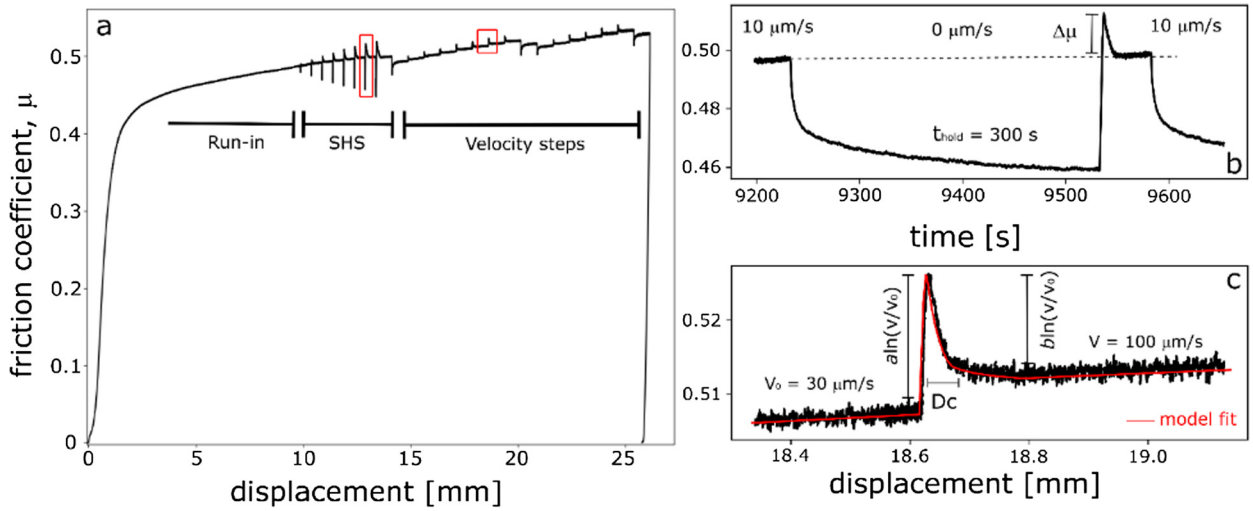

Fig. 2. a) Evolution of friction as a function of shear displacement for one complete experiment (b989). Our procedure consisted of a run-in phase followed by slide-hold-slide tests (SHS) and velocity step tests. b) Detail of a 300-s slide-hold-slide test showing evolution of friction with hold time and re-shear. c) Detail of a velocity step test from 30 to 100 s (black line) and a best-fit model using RSF (red line) (see text for details).

The experiments were performed at room temperature and at normal stress of 25, 50, 75 and 100 MPa for gouges and 10, 25, 35 and 50 MPa for intact wafers. We report on a total of 24 experiments (details in Table 2) with several other tests done to check consistency and perform calibrations. All experiments were performed under water saturated conditions by placing the experimental assembly within a plastic membrane and submerging it with $CaCO_3$-rich water. To ensure water percolation and full sample saturation, the samples were left under a low normal load of 1 kN for 30 minutes. After sample saturation, we increased the normal stress at steps of 0.4 MPa until the target normal stress was reached. Once the sample compacted to a constant layer thickness, during the run-in, the sample was sheared for 10 mm by imposing a displacement rate of 10 μm/s. During this phase, the fault reaches a steady state shear strength (Fig. 2a). After the run-in, we performed slide-hold-slide tests consisting of a shearing phase at 10 μm/s for 500 μm of displacement, alternated with hold periods ranging from 1 to 3000 s (Fig. 2b). Finally, we performed velocity steps by shearing the sample at increasing velocity, from 0.1 to 300 μm/s (Fig. 2c).

Our friction measurements include steady-state sliding friction, healing behaviour during slide-hold-slide tests, and velocity/state dependence of friction. The Rate and State friction theory (Dieterich, 1979; Ruina, 1983) is used as framework for this analysis (Fig. 2). The steady state friction coefficient (μ) was calculated as the shear stress normal stress ratio, and assuming negligible cohesion.

$$\mu_{ss} = \tau_{ss}/\sigma n \quad (1)$$

During slide-hold-slide tests, the amount of frictional healing ($\Delta\mu$) was calculated as the difference between the peak friction measured upon re-shear after each hold and the pre-hold steady state friction (Marone, 1998). Frictional healing rate (β) was calcu-

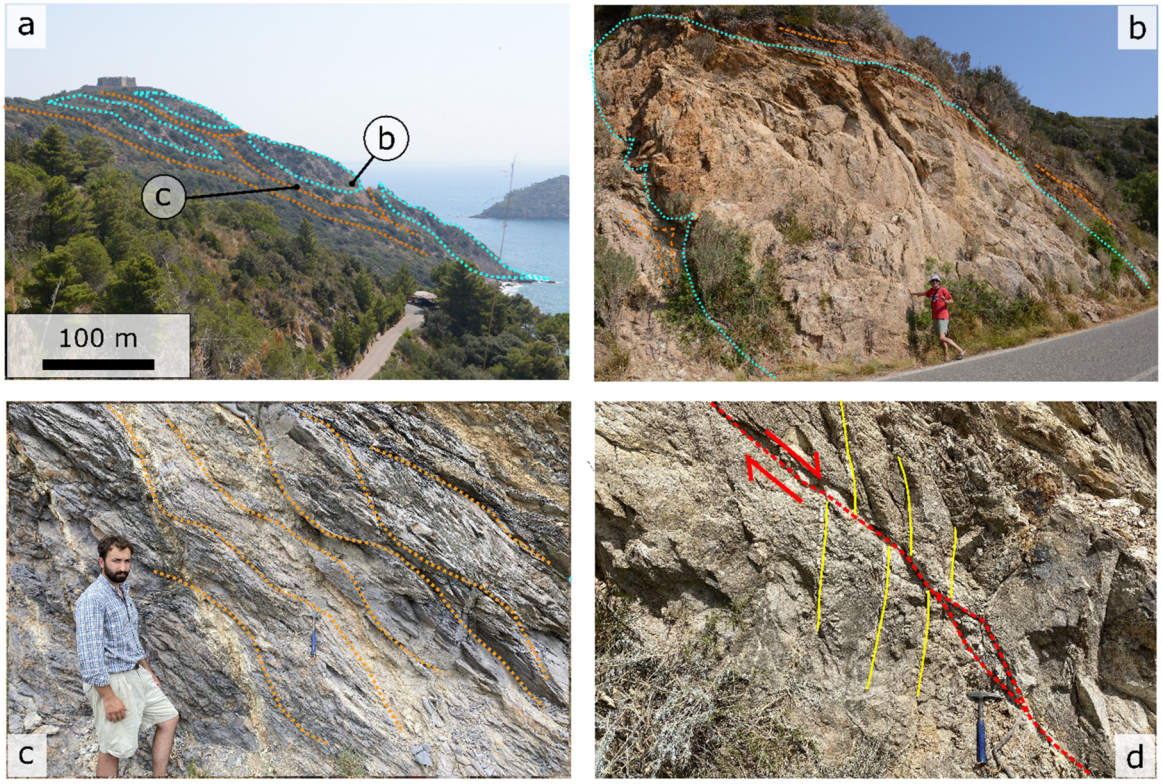

Fig. 3. Verrucano outcrops in Monte Argentario (see location in Fig. 1). a) panoramic view of the area, blue dotted lines highlight Anageniti lenses contained within the Scisti Viola matrix (foliation in brown dotted lines). b) decametric lens of Anageniti embedded with foliated Scisti Viola (brown dotted lines). c) Distributed deformation within the foliated (brown dotted line) Scisti Viola. d) Brittle fault within an Anageniti lens, yellow lines highlight subvertical quartz veins cut and displaced by the fault.

lated by diving the frictional healing ($\Delta\mu$) by the logarithm of the hold time, $\log_{10}(\Delta t)$.

$$\beta = \Delta\mu / \log_{10}(\Delta t). \quad (2)$$

During velocity steps test, the near-instantaneous step in sliding velocity from V_0 to V corresponds to an instantaneous change in friction that scales as the friction parameter $a\ln(V/V_0)$, where a is an empirical constant defined as the direct effect. The subsequent evolution to a new steady-state value of friction scales as the friction parameter $b\ln(V/V_0)$, where b is an empirical constant defined as the evolution effect (Dieterich, 1979; Ruina, 1983). The velocity dependence of friction, described by the a-b parameter, is defined as:

$$(a\text{-}b) = \Delta\mu_{ss} / \ln(V/V_0) \quad (3)$$

where $\Delta\mu_{ss}$ is the difference between the dynamic steady-state friction after and before a change in sliding velocity from V_0 to V (Dieterich, 1979; Ruina, 1983). Positive values of (a-b) define velocity-strengthening behaviour, indicating that aseismic creep is expected. Negative values of (a-b) define velocity-weakening behaviour, which is a condition required to develop a frictional instability (Dieterich and Kilgore, 1994; Marone, 1998). The velocity steps were modelled (Fig. 2c) using the Dieterich time-dependent evolution law coupled with the RSF equation (Dieterich, 1979):

$$\mu = \mu_0 + a\ln(V/V_0) + b\ln(V\theta/Dc) \quad (4)$$

$$\delta\theta/\delta t = 1 - \theta V/Dc \quad (5)$$

Where μ_0 is friction for steady-state slip at velocity V_0, V is the frictional slip rate and Dc is the critical slip distance needed to renew the asperities. Parameter θ, also calculated as Dc/V at steady state, represents the state variable that describes the average lifetime of the asperities (Ruina, 1983). For modelling, these two equations are coupled with an equation that describes the elastic coupling between the frictional surface and the loading surrounding:

$$d\mu/dt = K(V_{lp} - V) \quad (6)$$

Where V_{lp} is the measured loading point velocity and K is the stiffness of the loading apparatus and the assembly, normalized by the normal stress, in units of coefficient of friction per displacement (Saffer and Marone, 2003). These last three equations (eq. (4), (5) and (6)) are simultaneously solved by using a fifth order Runge-Kutta numerical integration. The constitutive parameters a, b, and Dc for each velocity step, were obtained as best fit parameter values using an iterative, least squares method to solve the nonlinear inverse problem (Blanpied et al., 1998; Saffer and Marone, 2003).

4. Results

4.1. Field work

One of the best exposures of the Verrucano formation, 500 m long and 250 m high, is located in Monte Argentario (Fig. 1 and Fig. 3). The outcrop consists of anastomosed and foliated phyllosilicate-rich rocks (Scisti Viola, Fig. 3a-c) that surround more competent quartz-rich sandstone and conglomerate lenses (Anageniti, Fig. 3b-d). The Scisti Viola are highly deformed domains characterized by phyllosilicate-rich pervasive foliation (details in paragraph 4.2) that obliterates the primary sedimentary features. In contrast to the Scisti Viola, the Anageniti are domains of lesser deformation that include places where the original sedimentary

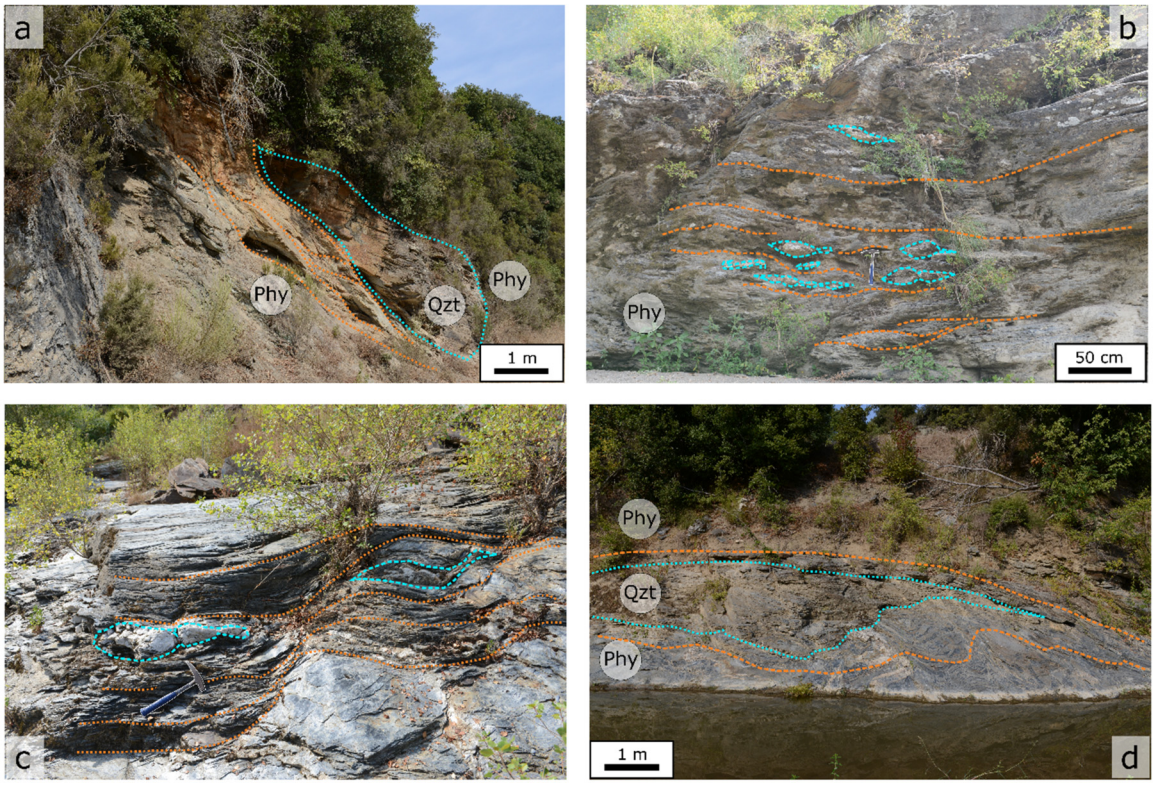

Fig. 4. Interpretation of outcrops of upper Palaeozoic basement in Monti Romani (see location in Fig. 1). a) Quartzite lens within foliated phyllite matrix. The boundary between the phyllites and the quartzites lens is marked by a distributed shear zone. b) Outcrop with the presence of strong quartz lenses surrounded by foliated phyllite matrix. c) Boudinated quartz lenses within a foliated phyllite matrix. d) Quartzite lens within phyllites foliated matrix. In circles: Phy is for phyllites, Qzt is for quartzites. Brown dashed lines marks foliation in phyllite matrix; light blue dashed lines encompass stronger quarts-rich lenses.

structures (e.g., stratification and pebbles imbrication) are preserved. Within the Anageniti we observed brittle features represented by different sets of quartz veins with a maximum thickness of 10 cm, veins of Fe and Mn oxides and minor faults with displacement lower than a few meters (Fig. 3d). Similar features have been observed in the Verrucano formation in eastern Elba, but here the geometries of the structures are not very well preserved. These features are obliterated by deformation that includes distributed Fe-rich mineralization and post-orogenic magmatism (Bortolotti et al., 2001; Smith et al., 2011).

We studied the upper Palaeozoic basement primarily in the Monti Romani area (Fig. 1 and details in Moretti et al., 1990). Here, phyllites alternate with fine grained quartzites (Fig. 4a) and, in some areas quartz-rich lenses are contained within an interconnected phyllosilicate-rich foliation (Fig. 4c-d and details in paragraph 4.2). In these outcrops the quartz-rich lenses range in size from centimetres to several meters. In some cases, brittle normal faults cut and displace the foliation, in others, normal faults mark the boundaries between the foliated matrix and the competent lenses (Fig. 4a).

4.2. Mineralogy and microstructures

XRD analysis provides semi-quantitative mineralogical analysis of the sampled basement rocks (Table 1). The composition is similar among the samples, which are mainly composed of quartz and phyllosilicates (muscovite and chlorite, with minor paragonite in upper Palaeozoic basement, and pyrophyllite in Anageniti). Minor mineral phases are oxides (rutile and hematite) and carbonates (calcite and dolomite).

Microstructural analysis was made on petrographic thin sections (30 μm thick) prepared by cutting the sampled rocks perpendicularly to foliation and parallel to the sense of shear. Images acquired using a petrographic microscope are reported in supplementary materials (Fig. S2). The sampled basement rocks show different microstructures that span between highly anisotropic (foliated) to isotropic (massive) textures. The Scisti Viola and upper Palaeozoic phyllites are characterized by a highly anisotropic texture due to pervasive plane-parallel foliation made of an alignment of phyllosilicate crystals that bound minor quartz microlithons (Fig. S2). Upper Palaeozoic quartzites show a schist-to-gneissic texture made of aligned phyllosilicate seams that envelop quartz-rich lenses. Anageniti is characterized by an isotropic, grain-supported texture made of sub-rounded quartz grains (up to several centimetres in diameter) with an interstitial non-foliated phyllosilicate matrix.

4.3. Mechanical results

For each lithology we have characterized frictional strength, healing rate and velocity dependence of friction (details in Table 2).

4.3.1. Frictional strength

During the run-in phase, the powdered material (blue curves in Fig. 5) reaches steady state friction with minor strain hardening trends, mostly appreciable in the Scisti Viola at high normal stresses (Fig. 5a). For wafers (red curves in Fig. 5c-d) we observe an initial, modest strain-weakening following the peak friction. The friction displacement curves for wafers are characterized by small oscillations while the curves for gouges are relatively smooth and steady.

The steady-state shear stress values for each lithology define a linear relation (Fig. 6) in agreement with Coulomb failure and cataclastic dominated processes and/or frictional sliding along phyllosilicate foliae. The steady state friction of the tested lithologies ranges between 0.19 and 0.52 (Table 2). Verrucano formation

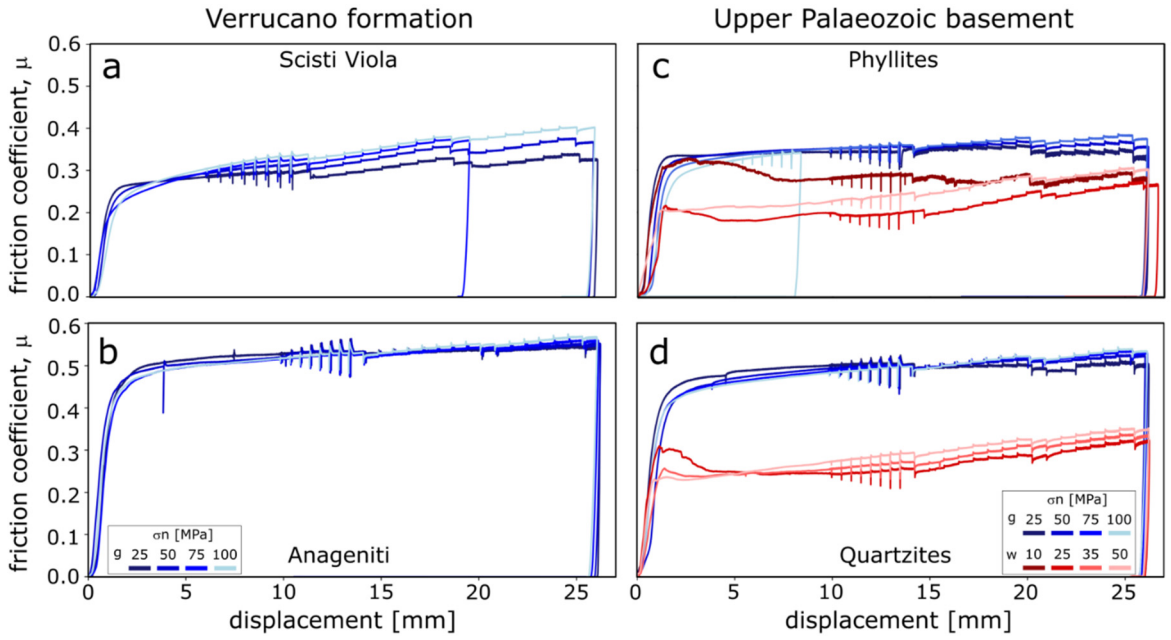

Fig. 5. Friction vs displacement curves for 22 experiments: gouge (p) results are shown in blue, wafers (w) results in red. Note that strain hardening occurs initially, after which, friction reaches a steady-state value for most of the experiments. See Table 2 for experiment details.

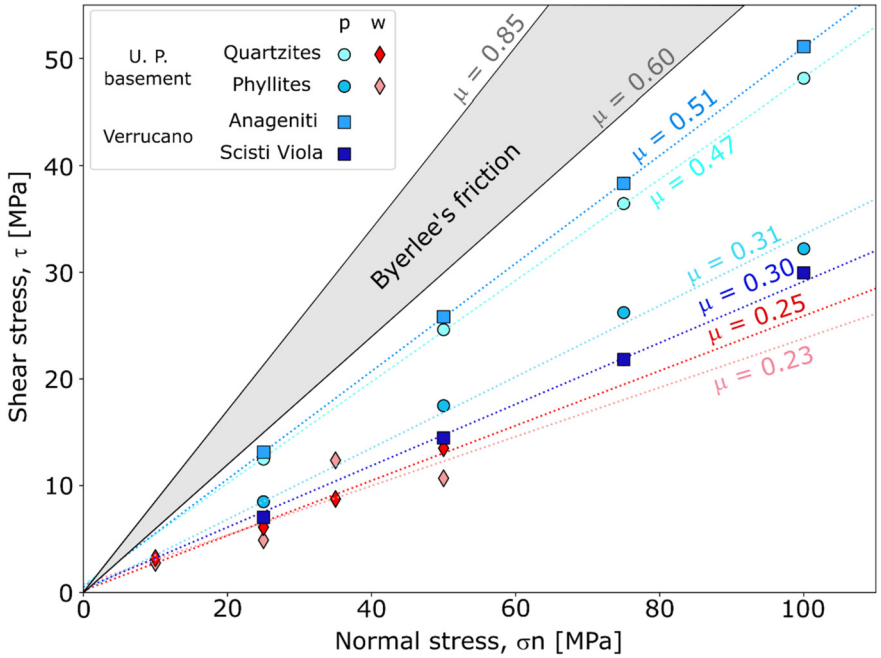

Fig. 6. Normal stress vs shear stress diagram of the tested lithologies: gouge (blues) and wafers (red diamonds). In grey the Byerlee range of friction (Byerlee, 1978). Data for both powdered and wafers plot along a linear trend in agreement with Coulomb failure and cataclastic dominated processes and/or frictional sliding along phyllosilicate foliae.

shows a large range in friction between the end member lithologies: for Scisti Viola $\mu = 0.30$ and for Anageniti $\mu = 0.51$. Concerning the upper Palaeozoic basement, powdered samples display $\mu = 0.31$ in phyllites and $\mu = 0.47$ in quartzites, whereas wafers samples show lower but similar fiction values in both lithologies: 0.23 for phyllites and 0.25 for quartzites.

4.3.2. Healing properties

Frictional restrengthening ($\Delta\mu$) shows different behaviour depending on the lithologies as well as the sample type (gouge and wafer). Within the Verrucano formation, Scisti Viola samples are characterized by small $\Delta\mu$ values that slightly increase with increasing hold time and normal stress (Fig. 7a). All the experiments conducted on Anageniti display a high healing rate that slightly decreases with normal stress ($\beta = 0.0074$ at 25 MPa and $\beta = 0.0068$ at 100 MPa, Fig. 7b). Within the upper Palaeozoic basement quartzite gouges have the highest values of $\Delta\mu$ which increase with hold time and slightly decrease with applied normal stress, maintaining an almost constant healing rate ($\beta = 0.0047$, Fig. 7d). The wafers of this lithology show lower values of frictional restrengthening resulting in lower healing rates ($\beta = 0.0014$, Fig. 7d). The phyllites of the upper Palaeozoic basement are characterized by low healing rates: $\beta = 0.0015$ and $\beta = 0.0005$ for gouges and wafers, respectively (Fig. 7c).

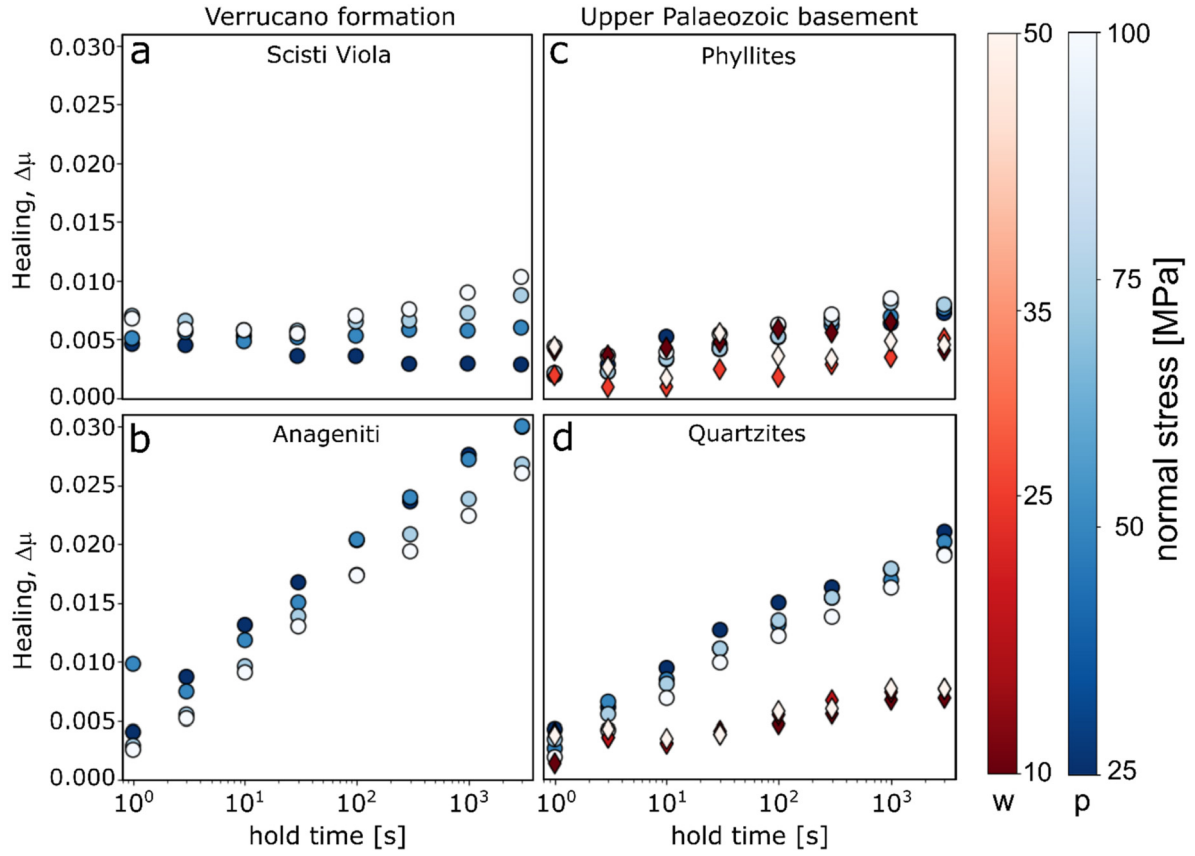

Fig. 7. Frictional healing, $\Delta\mu$, as function of hold time and applied normal stress: Triassic Verrucano left column, upper Palaeozoic basement right column. Circles for gouge (p) and diamonds for wafers (w). Note that the quartz dominated lithologies (Anageniti and Quartzites gouge) have the higher slopes, i.e., higher healing rates (details are reported in Table 2).

4.3.3. Velocity dependence of friction

The velocity dependence of friction for the Verrucano formation is strongly controlled by lithology. Scisti Viola gouges have the strongest velocity strengthening behaviour with *a-b* values that increase with increasing sliding velocities, i.e., *a-b* evolves from 0.002 to 0.004 (Fig. 8a). The Anageniti gouges show the lowest value of *a-b* around 0.0002, with a reduction in *a-b* values with decreasing normal stress (Fig. 8b). Gouges and wafers of the upper Palaeozoic phyllites and quartzites (Fig. 8c-d) are characterized by a velocity strengthening behaviour that increases with increasing sliding velocities. A few slightly negative *a-b* values were documented for phyllite gouges at 25 MPa of normal stress and shearing velocities in the range of 10-100 μm/s (Fig. 8c).

5. Discussion

5.1. Mineralogy, fabric and mechanical data

The integration of mineralogical and mechanical data highlights key aspects of two main rock types with different mechanical behaviour within the Apenninic basement: I) phyllosilicate-rich rocks represented by Scisti Viola and upper Palaeozoic phyllites characterized by 46% and 58% of muscovite and chlorite respectively; and II) quartz-rich rocks with about 65% of quartz, and minor phyllosilicates (i.e., Anageniti and quartzites, details in Table 1). The phyllosilicate-rich lithologies are characterized by low friction, $\mu \approx 0.3$ (Fig. 6), very low healing rates ($-0.0006 < \beta < 0.0017$, Fig. 7) and a marked velocity strengthening behaviour that increases with increasing sliding velocity (Fig. 8a-c). This behaviour is well-explained by the large amount of phyllosilicates contained within the phyllites and Scisti Viola that, during deformation, promotes the development of an interconnected network of phyllosilicates (Fig. 3c and Ruggieri et al., 2021) Frictional sliding along the phyllosilicate foliae favours low friction (e.g., Saffer and Marone, 2003; Moore and Lockner, 2004; Tembe et al., 2010; Ikari et al., 2011; Collettini et al., 2019), while the platy habit of the phyllosilicate affects the low healing and the marked velocity strengthening behaviour. This has been interpreted as a saturation of contact area for weak phyllosilicates at normal stresses above $\sim$ 25 MPa and for longer hold periods and lower slip velocity (Saffer and Marone, 2003; Ikari et al., 2009; Carpenter et al., 2011; Collettini et al., 2011; Tesei et al., 2012). We suggest that this observation is the result of a transition from phyllosilicate-dominated behaviour at low normal stress to a more pronounced quartz grains contact interaction, with some growth in contact area of quartz grains promoting the observed increase of β.

The quartz-dominated rocks of the Verrucano, and upper Palaeozoic basement show a relatively high friction coefficient $\mu \approx 0.5$ (Fig. 6), high healing rates ($0.0047 < \beta < 0.0076$, Fig. 7b-d) and a velocity strengthening behaviour that, for Anageniti evolves into a velocity neutral behaviour with decreasing normal stress (Fig. 8b). Here the mechanical data are mainly controlled by the large amount of quartz contained within these rocks. Cataclastic deformation with grain-size reduction and dilation well explains the high friction and the velocity strengthening behaviour (e.g., Marone and Scholz, 1988; Scholz, 1998), whereas the high healing rates are consistent with the increase of grain contact junctions with hold time (e.g., Dieterich and Kilgore, 1994; Marone, 1998). With increasing normal stress, we observe a reduction in frictional healing (Fig. 7b) and a more pronounced velocity strengthening behaviour (Fig. 8b). We interpret this as an increase in contact area saturation, either promoted by a quick saturation of quartz

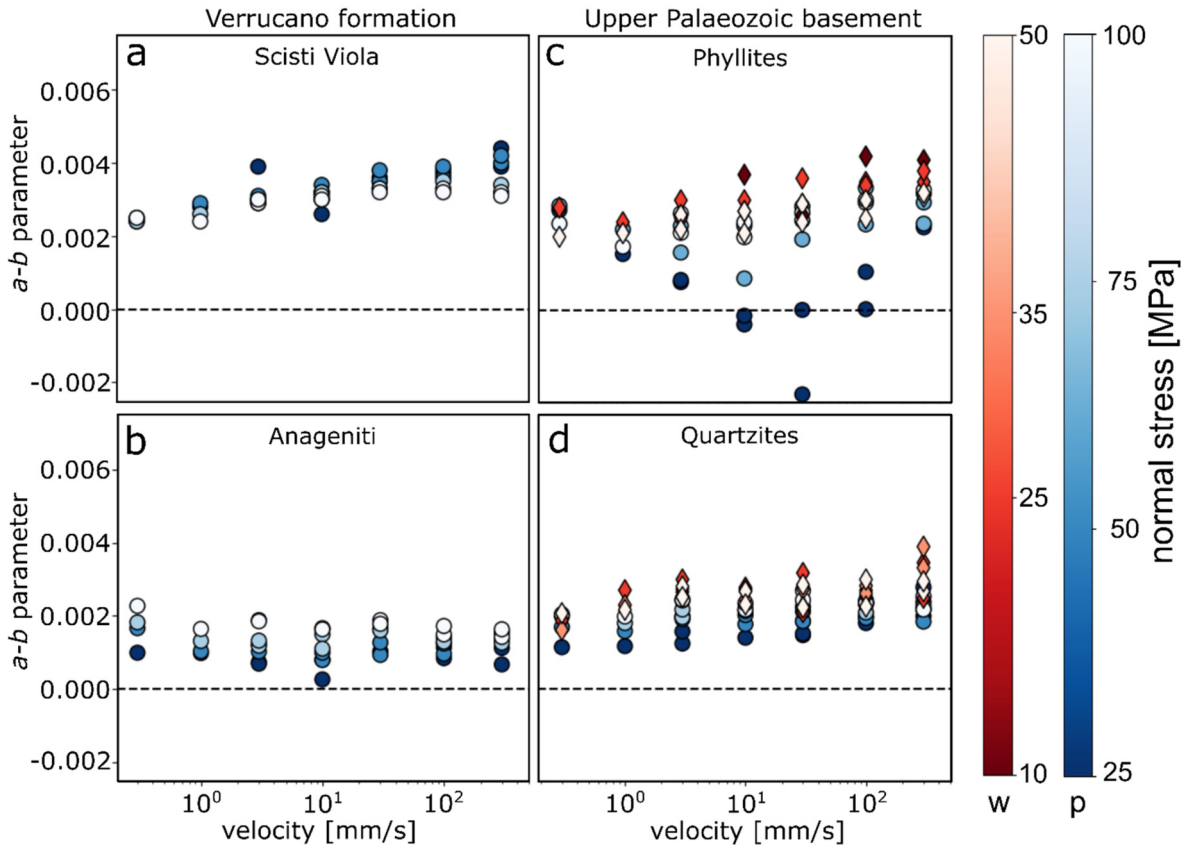

Fig. 8. Velocity dependence of friction, *a-b*, for the tested rocks: Triassic Verrucano left column, upper Palaeozoic basement right column. Circles for gouges (p) and diamonds for wafers (w). All the materials are characterized by a velocity strengthening behaviour (positive *a-b*). Wafers samples show the largest velocity strengthening behaviour that increases with increasing sliding velocity. Velocity strengthening decreases for Anageniti at lower normal stresses.

grain contacts at higher normal stresses (e.g., Ruggieri et al., 2021) and/or phyllosilicate enrichment within the shear zones.

Mechanical tests on wafers have been conducted only for foliated rock of the upper Palaeozoic basement. Despite the significant differences in phyllosilicates content, (i.e., 58% for phyllites and 33% for quartzites), their mechanical behaviour is very similar, and it is also similar to phyllosilicate-rich powdered samples (e.g., Fig. 6). In particular, friction is low, $0.23 < \mu < 0.25$, healing rate is close to zero ($0.0003 < \beta < 0.0014$), and a marked rate-strengthening behaviour is observed (Fig. 8c-d). In addition, the comparison of powdered vs. foliated quartzites shows completely different frictional properties, although mineralogical composition is the same. This result agrees with previous works showing that weakness of the foliated fault rocks is due to the reactivation of pre-existing phyllosilicate-rich surfaces that are absent in the powders (e.g., Collettini et al., 2009; Niemeijer et al., 2010). This observation emphasizes the role of fabric in frictional properties of phyllosilicate-rich rocks.

5.2. Structural and frictional properties of the basement and seismicity cut-off

Although the role of basement in the seismicity cut-off has been observed for the Colfiorito 1997 (Mirabella et al., 2008), L'Aquila 2009 (Baccheschi et al., 2020) and Emilia 2012 (Govoni et al., 2014) seismic sequences, the 2016-2017 Central Italy sequence is the best example to capture insights on fault rheology via the comparison between seismological, geological, and experimental mechanical data. For this seismic sequence, comprehensive seismological catalogues, based on machine learning techniques are available (e.g., Tan et al., 2021) and subsurface geology is constrained by seismic profiles and borehole data (Porreca et al., 2018; Barchi et al., 2021; Buttinelli et al., 2021). The sequence is characterized by three major earthquakes, the Mw 6.0 Amatrice event on 24th August 2016, the Mw 5.9 Visso event on 26th October and the Mw 6.5 Norcia event on 30th October. These events occurred on SW-dipping normal faults and details on fault geometry and kinematics can be found in the literature (Chiaraluce et al., 2017; Improta et al., 2019; Michele et al., 2020; Tan et al., 2021; Waldhauser et al., 2021). Along a crustal section that is parallel to the strike (147°, see trace in Fig. 1a) of the Norcia, Mw 6.5, mainshock (Chiaraluce et al., 2017), the aftershock distribution is mainly confined at depth < 9-10 km (Fig. 9). In addition, co-seismic fault slip distribution (Chiaraluce et al., 2017; Scognamiglio et al., 2018), shows that all the slip along the faults hosting the mainshocks is confined within the first 10 km of depth. At depth greater than 6 km, i.e., below the mainshock nucleation, the seismicity is concentrated on 2-4 km thick, sub-horizontal and imbricated bands (Fig. 9a). Different interpretations have been proposed for this basal seismicity. On the grounds of aftershock geometry and extensional focal mechanisms, Chiaraluce et al. (2017) interpret this seismicity as a basal extensional shear zone that in some places is fragmented (Waldhauser et al., 2021). From the imbrication of the basal seismicity bands, Improta et al. (2019) suggested a reactivation of previously developed compressional structures that root into the basement. Here, building on the observation that the bottom of the basal seismicity coincides with the top of the basement (Fig. 9), we propose that this seismicity cut-off is mainly controlled by the basement rheology.

Significant insights into the rheology of the basement can be obtained from the geological and mechanical investigations reported in this paper. The studied outcrops of the Verrucano for-

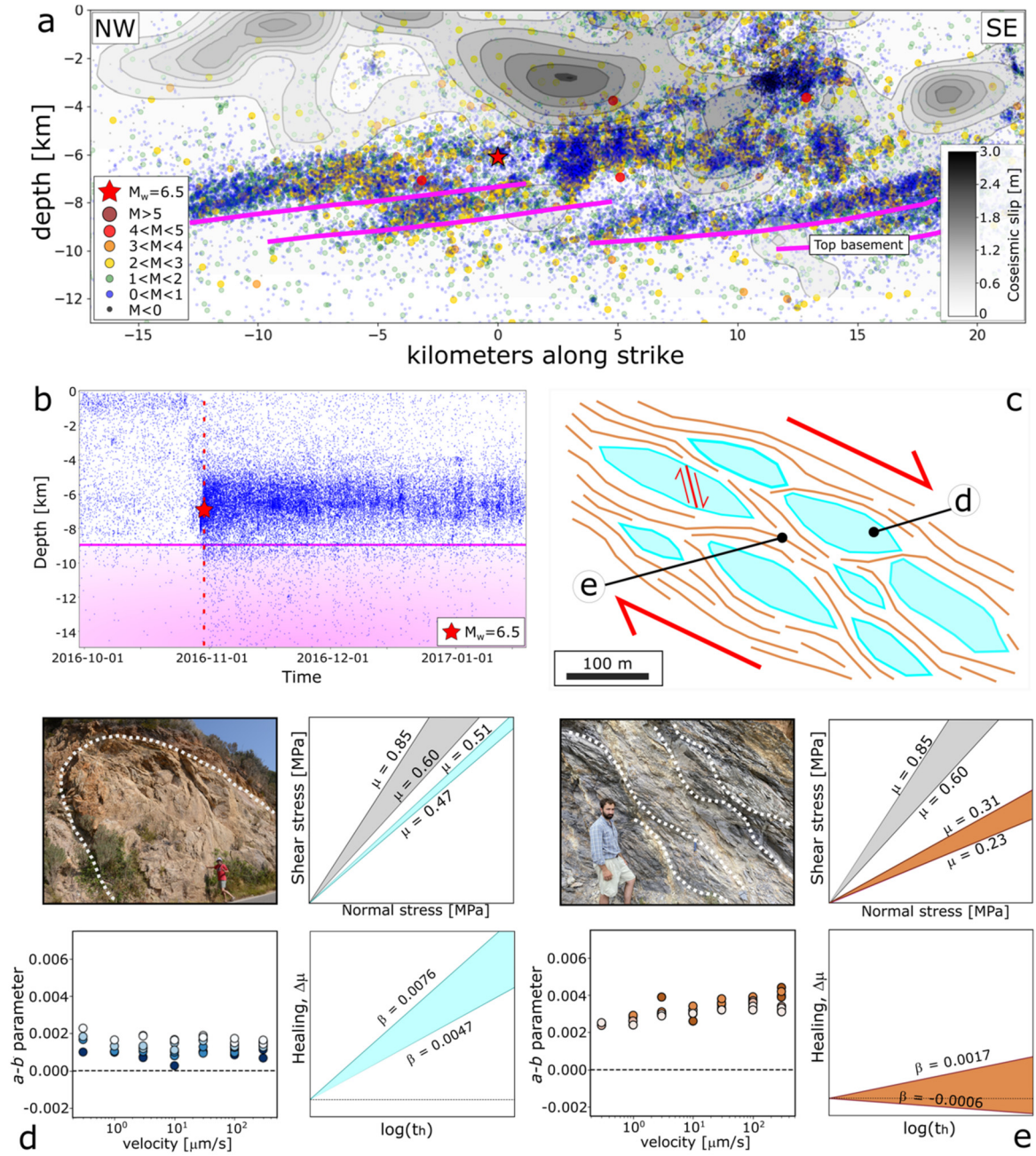

Fig. 9. The road to integration for the role of basement in the seismicity cut-off of the Apennines. a) vertical cross section (see trace in Fig. 1a) parallel to the strike of Norcia, Mw = 6.5 mainshock, integrating seismicity recorded in the 20 days following the mainshock (Tan et al., 2021): all events within 2 km from the cross-section vertical plane are shown. In-depth geometry of the basement (purple lines) is reconstructed on the grounds of seismic profiles and borehole data (Barchi et al., 2021). Co-seismic slip is in grey scale (Scognamiglio et al., 2018 and Chiaraluce et al., 2017). b) Depth-time seismicity distribution in proximity of the Norcia mainshock (red star and dotted line) along the same longitudinal section presented in panel a. The purple line indicates the average depth of the basement. c) Schematic representation for a basement shear zone: this reconstruction is based on the geological interpretation of Fig. 3a, and details reported in panel d and e. Quartz-rich lenses in light blue and structural and mechanical details in panel d. Interconnected phyllosilicate-rich horizons in brown and structural and mechanical details in panel e.

mation and upper Palaeozoic basement rock schematically consist of interconnected networks of foliated and phyllosilicate-rich horizons (the Scisti Viola in the Verrucano and the phyllites in the upper Palaeozoic basement) that surround more competent quartz-rich lithologies (Anageniti in Verrucano and quartzites in the upper Palaeozoic basement). Due to their interconnectivity (Fig. 9c), the phyllosilicate-rich horizons control the rheology of the basement. These rocks are characterized by low friction, very low or null healing rates, and a marked rate strengthening behaviour (Fig. 9e). These data define the basement as a several kilometres thick, weak layer, which accommodates deformation predominantly by aseismic creep. In other words, the basement is a good horizon for a frictionally controlled seismicity cut-off. The seismicity, above the phyllitic basement is well explained, on the other hand, by the frictional properties of the carbonates-anhydrites rich faults hosted within the sedimentary cover (high-friction, velocity neutral-weakening behaviour and high healing rates; Scuderi et al., 2013; Carpenter et al., 2014; Scuderi et al., 2020).

Our results suggest that the documented seismicity cut-off is frictionally controlled and does not correspond to the canonical brittle-ductile transition, BDT, i.e., a transition zone where the deformation switches from frictional faulting along brittle structures

to viscous shearing in thick mylonites once achieved a temperature of about 300-350 °C (Brace and Kohlstedt, 1980; Wallis et al., 2015). Firstly, the maximum depth of the background microseismicity, which defines the base of the seismogenic regime (e.g., Sibson, 1989; Scholz, 2019) or the canonical BDT, is located at 14-15 km in this portion of the Apennines (Chiaraluce et al., 2017). Secondly, a new heat flow map built on the temperature data from 174 boreholes poses the modelled BDT at depths between 15-20 km (Pauselli et al., 2019). Thirdly, frictional sliding of muscovite-rich phyllosilicates is favoured up to temperatures as high as 600 °C (Den Hartog et al., 2013). These temperatures are significantly higher than the 200 °C expected at 10 km depth in the active portion of the Apennines (Pauselli et al., 2019), indicating that brittle frictional sliding is the main deformation mechanism for basement rocks at these depths. Finally, the seismicity cut-off is not planar (Fig. 9a-b), as it should be for a temperature-controlled cut-off, but it rather mimics the basal geometry of the major thrusts of the area that are imbricated and root into the basement (Fig. 9a and Barchi et al., 2021).

Following the Norcia 30th October mainshock, an increment of diffuse microseismicity is observed within the basement (Fig. 9a-b). A possible explanation for that is found in the structural and frictional heterogeneous nature of the basement. Within the basement we have documented the presence of quartz-rich lenses, with size ranging from centimetres to hundreds of meters (e.g., Fig. 9c, 3 and 4), showing brittle structures such as faults with small displacement and veins (Fig. 3). These rocks are characterized by relatively high friction, high healing rates, and a velocity strengthening/neutral behaviour. The quartz-rich lenses are therefore strong and competent objects interspersed within the weak foliated phyllosilicate-rich matrix (Fig. 9c). Lithological heterogeneity promotes differences in strain rate and finite strain magnitude (e.g., Goodwin and Tikoff, 2002) with local strain rate gradients that induce amplified shear stresses in the competent lenses (Beall et al., 2019). During tectonic loading, shear strain-rate increase can result in amplified shear stresses along the competent lenses and trigger a dynamic instability also in a slightly velocity strengthening/neutral material (e.g., Boatwright and Cocco, 1996) like those represented by quartz-rich lenses hosted within the basement. Therefore, we interpret that the deep microseismicity following the Norcia mainshock (Fig. 9b) originates from these competent lenses, which deform in response to the post-seismic increase of shear strain rate. The seismicity located within the basement is mainly characterized by $M < 2.0$ earthquakes (Fig. 9a) with a few events in the range $2.0 < M < 4.0$. The $0 < M < 2.0$ events represent ruptures with dimensions ranging from 10 to about 300 m (Sibson, 1989) that is the same scale of the competent lenses observed in the field (Fig. 9c-d). The few larger ruptures can be explained via the interaction of several competent lenses forming force chains that are activated simultaneously (e.g., Fagereng and Beall, 2021) or by basement portions with rheology not entirely dominated by phyllosilicates.

6. Conclusions

In the active region of the Apennines, the integration of seismic reflection profiles with high resolution seismological data shows that the strongest seismic sequences are confined within the sedimentary cover. For the Amatrice-Norcia 2016 seismic sequence the integration of geophysical data highlights a seismicity cut-off at 9-10 km of depth in correspondence of the top of the basement that shows several steps produced during the Pliocene compressional tectonic phase. Outcrops of exhumed basement rocks schematically consist of structural and mechanical heterogeneous zones of distributed deformation along interconnected phyllosilicate-rich horizons surrounding quartz-rich lenses up to hundred meters thick. Due to their interconnectivity, the rheology of the basement is controlled by the phyllosilicate-rich horizons. These rocks show low friction, $0.23 < \mu < 0.31$, very low or null healing rates, $-0.0006 < \beta < 0.0017$, and marked rate strengthening behaviour. The integration of field and laboratory data depicts the basement as a several kilometre thick, weak layer, which accommodates deformation predominantly by aseismic creep, hence representing a good horizon for a frictionally controlled seismicity cut-off. Following the mainshock, the increase of seismic activity at higher depths (i.e., within the basement) is interpreted as the brittle reactivation of quartz-rich competent lenses following post-mainshock shear strain rate increase. The integration of subsurface geology and seismological data with structural observations and friction experiments on rocks that represent exhumed analogues of those present at seismogenic depths depict a model in which the depth of the seismogenic zone is dictated by the frictional, rate-strengthening properties of basement rocks.

CRediT authorship contribution statement

G.V., G.P. and C.C. wrote the main manuscript text. G.V. and G.P. worked on the experimental dataset. G.V., G.P., E.C. and C.C. carried the field work. L.A. performed mineralogical analysis. E.T., M.R.B., C.C., E.C. and G.V. worked on the geophysical data. M.M.S, C.C., G.P., and C.M. supervised the experimental analysis. G.V. and G.P prepared the figures. All authors reviewed the manuscript.

Declaration of competing interest

The authors declare that they have no known competing financial interests or personal relationships that could have appeared to influence the work reported in this paper.

Acknowledgement

We thank T. Tesei for discussions regarding this work and N. Bigaroni for assistance during experimental procedures. We also thank dr. P. Scarlato for support at the INGV HP-HT laboratory, dr. D. Mannetta for his help with sample preparation. This research was supported by ERC grant Nr. 259256 GLASS and Ateneo 2018 to C. Collettini and ERC grant TECTONIC Nr. 835012 to C. Marone.

Appendix A. Supplementary material

Supplementary material related to this article can be found online at https://doi.org/10.1016/j.epsl.2022.117444.

References

Aldinucci, M., Gandin, A., Sandrelli, F., 2008. The Mesozoic continental rifting in the Mediterranean area: insights from the Verrucano tectofacies of southern Tuscany (Northern Apennines, Italy). Int. J. Earth Sci. 97 (6), 1247–1269.

Anderlini, L., Serpelloni, E., Belardinelli, M.E., 2016. Creep and locking of a low-angle normal fault: insights from the Altotiberina fault in the northern Apennines (Italy). Geophys. Res. Lett. 43 (9), 4321–4329.

Anelli, L., Gorza, M., Pieri, M., Riva, M., 1994. Subsurface well data in the Northern Apennines (Italy). Mem. Soc. Geol. Ital. 48, 461–471.

Avouac, J.P., 2015. From geodetic imaging of seismic and aseismic fault slip to dynamic modelling of the seismic cycle. Annu. Rev. Earth Planet. Sci. 43, 233–271.

Baccheschi, P., De Gori, P., Villani, F., Trippetta, F., Chiarabba, C., 2020. The preparatory phase of the Mw 6.1 2009 L'Aquila (Italy) normal faulting earthquake traced by foreshock time-lapse tomography. Geology 48 (1), 49–55.

Bally, A.W., Burbi, L., Cooper, C., Ghelardoni, R., 1986. Balanced cross-sections and seismic reflection profiles across the central Apennines. Mem. Soc. Geol. Ital. 35, 257–310.

Barchi, M.R., Collettini, C., 2019. Seismicity of central Italy in the context of the geological history of the Umbria-Marche Apennines. In: Koeberl, C., Bice, D.M. (Eds.), 250 Million Years of Earth History in Central Italy: Celebrating 25 Years of the Geological Observatory of Coldigioco, Vol. 542. Geological Society of America Special Paper, pp. 175–190.

Barchi, M.R., De Feyter, A., Magnani, M.B., Minelli, G., Pialli, G., Sotera, M., 1998. The structural style of the Umbria-Marche fold and thrust belt. Mem. Soc. Geol. Ital. 52, 557–578.
Barchi, M.R., Carboni, F., Michele, M., Ercoli, M., Giorgetti, C., Porreca, M., Azzaro, S., Chiaraluce, L., 2021. The influence of subsurface geology on the distribution of earthquakes during the 2016—2017 Central Italy seismic sequence. Tectonophysics 807, 228797.
Baumberger, T., Heslot, F., Perrin, B., 1994. Crossover from creep to inertial motion in friction dynamics. Nature 367 (6463), 544–546.
Beall, A., Fagereng, Å., Ellis, S., 2019. Strength of strained two-phase mixtures: application to rapid creep and stress amplification in subduction zone mélange. Geophys. Res. Lett. 46 (1), 169–178.
Bedford, J.D., Faulkner, D.R., 2021. The role of grain size and effective normal stress on localization and the frictional stability of simulated quartz gouge. Geophys. Res. Lett. 48 (7), e2020GL092023.
Beeler, N.M., Tullis, T.E., Blanpied, M.L., Weeks, J.D., 1996. Frictional behavior of large displacement experimental faults. J. Geophys. Res., Solid Earth 101 (B4), 8697–8715.
Blanpied, M.L., Marone, C.J., Lockner, D.A., Byerlee, J.D., King, D.P., 1998. Quantitative measure of the variation in fault rheology due to fluid-rock interactions. J. Geophys. Res., Solid Earth 103 (B5), 9691–9712.
Boatwright, J., Cocco, M., 1996. Frictional constraints on crustal faulting. J. Geophys. Res., Solid Earth 101 (B6), 13895–13909.
Bortolotti, V., Fazzuoli, M., Pandeli, E., Principi, G., Babbini, A., Corti, S., 2001. Geology of central and eastern Elba Island, Italy. Ofioliti 26 (2a), 97–150.
Brace, W.F., Kohlstedt, D.L., 1980. Limits on lithospheric stress imposed by laboratory experiments. J. Geophys. Res., Solid Earth 85 (B11), 6248–6252.
Bürgmann, R., 2018. The geophysics, geology and mechanics of slow fault slip. Earth Planet. Sci. Lett. 495, 112–134.
Buttinelli, M., Petracchini, L., Maesano, F.E., D'Ambrogi, C., Scrocca, D., Marino, M., Capotorti, F., Bigi, S., Cavinato, G.P., Mariucci, M.T., Montone, P., Di Bucci, D., 2021. The impact of structural complexity, fault segmentation, and reactivation on seismotectonics: constraints from the upper crust of the 2016–2017 Central Italy seismic sequence area. Tectonophysics 810, 228861.
Byerlee, J., 1978. Friction of rocks. Pure Appl. Geophys. 116, 615–626.
Cappa, F., Scuderi, M.M., Collettini, C., Guglielmi, Y., Avouac, J.P., 2019. Stabilization of fault slip by fluid injection in the laboratory and in situ. Sci. Adv. 5 (3), eaau4065.
Carminati, E., Doglioni, C., 2012. Alps vs. Apennines: the paradigm of a tectonically asymmetric Earth. Earth-Sci. Rev. 112 (1–2), 67–96.
Carminati, E., Lustrino, M., Doglioni, C., 2012. Geodynamic evolution of the central and western Mediterranean: tectonics vs. igneous petrology constraints. Tectonophysics 579, 173–192.
Carpenter, B.M., Marone, C., Saffer, D.M., 2011. Weakness of the San Andreas Fault revealed by samples from the active fault zone. Nat. Geosci. 4 (4), 251–254.
Carpenter, B.M., Scuderi, M.M., Collettini, C., Marone, C., 2014. Frictional heterogeneities on carbonate-bearing normal faults: Insights from the Monte Maggio Fault, Italy. J. Geophys. Res., Solid Earth 119 (12), 9062–9076.
Cassinis, G., Perotti, C., Santi, G., 2018. Post-Variscan Verrucano-like deposits in Italy, and the onset of the alpine tectono-sedimentary cycle. Earth-Sci. Rev. 185, 476–497.
Centamore, E., Deiana, G., Micarelli, A., Potetti, M., 1986. Il Trias-Paleogene delle Marche.
Chen, W.P., Molnar, P., 1983. Focal depths of intracontinental and intraplate earthquakes and their implications for the thermal and mechanical properties of the lithosphere. J. Geophys. Res., Solid Earth 88 (B5), 4183–4214.
Chiarabba, C., Amato, A., Anselmi, M., Baccheschi, P., Bianchi, I., Cattaneo, M., Cerere, G., Chiaraluce, L., Ciaccio, M.G., De Gori, P., De Luca, G., Di Bona, M., Di Stefano, R., Faenza, L., Govoni, A., Improta, L., Lucente, F.P., Marchetti, A., Margheriti, L., Mele, F., Michelini, A., Monachesi, G., Moretti, M., Pastori, M., Piana Agostinetti, N., Piccinini, D., Roselli, P., Seccia, D., Valoroso, L., 2009. The 2009 L'Aquila (central Italy) MW6.3 earthquake: main shock and aftershocks. Geophys. Res. Lett. 36 (18).
Chiarabba, C., De Gori, P., Improta, L., Lucente, F.P., Moretti, M., Govoni, A., Di Bona, M., Margheriti, L., Marchetti, A., Nardi, A., 2014. Frontal compression along the Apennines thrust system: the Emilia 2012 example from seismicity to crustal structure. J. Geodyn. 82, 98–109.
Chiaraluce, L., Ellsworth, W.L., Chiarabba, C., Cocco, M., 2003. Imaging the complexity of an active normal fault system: the 1997 Colfiorito (central Italy) case study. J. Geophys. Res. 108 (B6). https://doi.org/10.1029/2002jb002166.
Chiaraluce, L., Chiarabba, C., Collettini, C., Piccinini, D., Cocco, M., 2007. Architecture and mechanics of an active low-angle normal fault: Alto Tiberina fault, northern Apennines, Italy. J. Geophys. Res., Solid Earth 112 (B10).
Chiaraluce, L., Barchi, M.R., Carannante, S., Collettini, C., Mirabella, F., Pauselli, C., Valoroso, L., 2017. The role of rheology, crustal structures and lithology in the seismicity distribution of the northern Apennines. Tectonophysics 694, 280–291.
Collettini, C., Barchi, M.R., 2002. A low-angle normal fault in the Umbria region (Central Italy): a mechanical model for the related microseismicity. Tectonophysics 359 (1–2), 97–115.
Collettini, C., Niemeijer, A., Viti, C., Marone, C.J., 2009. Fault zone fabric and fault weakness. Nature 462, 907–910.
Collettini, C., Niemeijer, A., Viti, C., Smith, S.A., Marone, C., 2011. Fault structure, frictional properties and mixed-mode fault slip behavior. Earth Planet. Sci. Lett. 311 (3–4), 316–327.
Collettini, C., Di Stefano, G., Carpenter, B., Scarlato, P., Tesei, T., Mollo, S., Trippetta, F., Marone, C., Romeo, G., Chiaraluce, L., 2014. A novel and versatile apparatus for brittle rock deformation. Int. J. Rock Mech. Min. Sci. 66, 114–123.
Collettini, C., Tesei, T., Scuderi, M.M., Carpenter, B.M., Viti, C., 2019. Beyond Byerlee friction, weak faults and implications for slip behavior. Earth Planet. Sci. Lett. 519, 245–263.
Cresta, S., Monechi, S., Parisi, G., 1989. Stratigrafia del mesozoico e cenozoico nell'area umbro-marchigiana. Mem. Descr. Carta Geol. Ital. 34, 185.
Den Hartog, S.A.M., Niemeijer, A.R., Spiers, C.J., 2013. Friction on subduction megathrust faults: beyond the illite–muscovite transition. Earth Planet. Sci. Lett. 373, 8–19.
Dieterich, J.H., 1979. Modeling of rock friction 1. Experimental results and constitutive equations. J. Geophys. Res., Solid Earth 84, 2161–2168. https://doi.org/10.1029/JB084iB05p02161.
Dieterich, J.H., Kilgore, B.D., 1994. Direct observation of frictional contacts: new insights for state-dependent properties. Pure Appl. Geophys. 143, 283–302. https://doi.org/10.1007/BF00874332.
Eyre, T.S., Eaton, D.W., Garagash, D.I., Zecevic, M., Venieri, M., Weir, R., Lawton, D.C., 2019. The role of aseismic slip in hydraulic fracturing–induced seismicity. Sci. Adv. 5 (8), eaav7172.
Fagereng, Å., Beall, A., 2021. Is complex fault zone behaviour a reflection of rheological heterogeneity? Philos. Trans. R. Soc. A 379 (2193), 20190421.
Goodwin, L.B., Tikoff, B., 2002. Competency contrast, kinematics, and the development of foliations and lineations in the crust. J. Struct. Geol. 24 (6–7), 1065–1085.
Govoni, A., Marchetti, A., De Gori, P., Di Bona, M., Lucente, F.P., Improta, L., Chiarabba, C., Nardi, A., Margheriti, L., Piana Agostinetti, N., Di Giovambattista, R., Latorre, D., Anselmi, M., Ciaccio, M.G., Moretti, M., Castellano, C., Piccinini, D., 2014. The 2012 Emilia seismic sequence (Northern Italy): imaging the thrust fault system by accurate aftershock location. Tectonophysics 622, 44–55.
Gu, Y., Wong, T.F., 1994. Nonlinear Dynamics of the Transition from Stable Sliding to Cyclic-Stick-Slip in Rock. Geophysical Monograph-American Geophysical Union, vol. 83, pp. 15-15.
Ikari, M.J., Saffer, D.M., Marone, C., 2009. Frictional and hydrologic properties of clay-rich fault gouge. J. Geophys. Res., Solid Earth 114 (B5).
Ikari, M.J., Marone, C., Saffer, D.M., 2011. On the relation between fault strength and frictional stability. Geology 39, 83–86. https://doi.org/10.1130/G31416.1.
Improta, L., Latorre, D., Margheriti, L., Nardi, A., Marchetti, A., Lombardi, A.M., Castello, B., Villani, F., Ciaccio, M.G., Mele, F.M., Moretti, M., 2019. Multi-segment rupture of the 2016 Amatrice-Visso-Norcia seismic sequence (central Italy) constrained by the first high-quality catalog of Early Aftershocks. Sci. Rep. 9 (1), 1–13.
Jolivet, R., Frank, W.B., 2020. The transient and intermittent nature of slow slip. AGU Adv. 1 (1), e2019AV000126.
Lazzarotto, A., Aldinucci, M., Cirilli, S., Costantini, A., Decandia, F.A., Pandeli, E., Sandrelli, F., Spina, A., 2003. Stratigraphic correlation of the Upper Palaeozoic-Triassic successions in southern Tuscany, Italy. Boll. Soc. Geol. Ital. 2, 25–35. Roma.
Leeman, J.R., Saffer, D.M., Scuderi, M.M., Marone, C., 2016. Laboratory observations of slow earthquakes and the spectrum of tectonic fault slip modes. Nat. Commun. 7 (1), 1–6.
Marone, C., 1998. Laboratory-derived friction laws and their application to seismic faulting. Annu. Rev. Earth Planet. Sci. 26, 643–696. https://doi.org/10.1146/annurev.earth.26.1.643.
Marone, C., 2019. The spectrum of fault slip modes from elastodynamic rupture to slow earthquakes. In: Bizzarri, A., Das, S., Petri, A. (Eds.), Proc. Internat. School of Physics "Enrico Fermi" on Mechanics of Earthquake Faulting. IOS Press, Amsterdam, the Netherlands, pp. 81–94.
Marone, C., Scholz, C.H., 1988. The depth of seismic faulting and the upper transition from stable to unstable slip regimes. Geophys. Res. Lett. 15 (6), 621–624.
Mclaskey, G.C., Yamashita, F., 2017. Slow and fast ruptures on a laboratory fault controlled by loading characteristics. J. Geophys. Res., Solid Earth 122 (5), 3719–3738.
Michele, M., Chiaraluce, L., Di Stefano, R., Waldhauser, F., 2020. Fine-scale structure of the 2016–2017 Central Italy seismic sequence from data recorded at the Italian National Network. J. Geophys. Res., Solid Earth 125, e2019JB018440. https://doi.org/10.1029/2019JB018440.
Mirabella, F., Barchi, M.R., Lupattelli, A., 2008. Seismic reflection data in the Umbria Marche region: limits and capabilities to unravel the subsurface structure in a seismically active area. Ann. Geophys. 51 (2–3), 383–396. https://doi.org/10.4401/ag-3032.
Montone, P., Mariucci, M.T., 2016. The new release of the Italian contemporary stress map. Geophys. J. Int. 205 (3), 1525–1531.
Montone, P., Mariucci, M.T., 2020. Constraints on the structure of the shallow crust in central Italy from geophysical log data. Sci. Rep. 10, 3834. https://doi.org/10.1038/s41598-020-60855-0.

Moore, D.E., Lockner, D.A., 2004. Crystallographic controls on the frictional behavior of dry and water-saturated sheet structure minerals. J. Geophys. Res., Solid Earth 109 (B3).
Moore, D.M., Reynolds Jr., R.C., 1997. X-Ray Diffraction and the Identification and Analysis of Clay Minerals. Oxford University Press, Oxford, UK, 378 pp.
Moretti, A., Meletti, C., Ottria, G., 1990. Studio stratigrafico e strutturale dei Monti Romani (GR-VT)-1: Dal Paleozoico all'orogenesi alpidica. Boll. Soc. Geol. Ital. 109 (3), 557–581.
Niemeijer, A., Marone, C., Elsworth, D., 2010. Fabric induced weakness of tectonic faults. Geophys. Res. Lett. 37 (3).
Pandeli, E., Gianelli, G., Puxeddu, M., Elter, F.M., 1994. The Paleozoic basement of the Northern Apennines: stratigraphy, tectonometamorphic evolution and Alpine hydrothermal processes. Mem. Soc. Geol. Ital. 48, 627–654. Roma.
Passelègue, F.X., Aubry, J., Nicolas, A., Fondriest, M., Deldicque, D., Schubnel, A., Di Toro, G., 2019. From fault creep to slow and fast earthquakes in carbonates. Geology 47 (8), 744–748.
Patacca, E., Scandone, P., Di Luzio, E., Cavinato, G.P., Parotto, M., 2008. Structural architecture of the central Apennines: interpretation of the CROP 11 seismic profile from the Adriatic coast to the orographic divide. Tectonics 27 (3).
Pauselli, C., Gola, G., Mancinelli, P., Trumpy, E., Saccone, M., Manzella, A., Ranalli, G., 2019. A new surface heat flow map of the Northern Apennines between latitudes 42.5 and 44.5 N. Geothermics 81, 39–52.
Perfettini, H., Avouac, J.P., Tavera, H., Kositsky, A., Nocquet, J.M., Bondoux, F., Chlieh, M., Sladen, A., Audin, L., Farber, D.L., Soler, P., 2010. Seismic and aseismic slip on the Central Peru megathrust. Nature 465 (7294), 78–81.
Pialli, G., 1998. Results of the CROP03 deep seismic reflection profile. Mem. Soc. Geol. Ital. 52, 657.
Ponziani, F., De Franco, R., Minelli, G., Biella, G., Federico, C., Pialli, G., 1995. Crustal shortening and duplication of the Moho in the Northern Apennines: a view from seismic refraction data. Tectonophysics 252 (1–4), 391–418.
Porreca, M., Minelli, G., Ercoli, M., Brobia, A., Mancinelli, P., Cruciani, F., Giorgetti, C., Carboni, C., Mirabella, F., Cavinato, G., Cannata, A., Pauselli, C., Barchi, M.R., 2018. Seismic reflection profiles and subsurface geology of the area interested by the 2016–2017 earthquake sequence (Central Italy). Tectonics 37, 1–22. https://doi.org/10.1002/2017TC004915.
Ruggieri, R., Scuderi, M.M., Trippetta, F., Tinti, E., Brignoli, M., Mantica, S., Petroselli, S., Osculati, L., Volontè, G., Collettini, C., 2021. The role of shale content and pore-water saturation on frictional properties of simulated carbonate faults. Tectonophysics 807, 228811.
Ruina, A., 1983. Slip instability and state variable friction laws. J. Geophys. Res. 88, 10359–10370. https://doi.org/10.1029/JB088iB12p10359.
Saffer, D.M., Marone, C., 2003. Comparison of smectite- and illite-rich gouge frictional properties: application to the updip limit of the seismogenic zone along subduction megathrusts. Earth Planet. Sci. Lett. 215 (1–2), 219–235.
Scholz, C.H., 1998. Earthquakes and friction laws. Nature 391 (6662), 37–42.
Scholz, C.H., 2019. The Mechanics of Earthquakes and Faulting. Cambridge University Press.
Scognamiglio, L., Tinti, E., Casarotti, E., Pucci, S., Villani, F., Cocco, M., Michelini, A., Dreger, D., 2018. Complex fault geometry and rupture dynamics of the MW 6.5, 30 October 2016, Central Italy earthquake. J. Geophys. Res., Solid Earth 123 (4), 2943–2964.
Scrocca, D., Carminati, E., Doglioni, C., 2005. Deep structure of the southern Apennines, Italy: thin-skinned or thick-skinned? Tectonics 24 (3).
Scuderi, M.M., Niemeijer, A.R., Collettini, C., Marone, C., 2013. Frictional properties and slip stability of active faults within carbonate–evaporite sequences: the role of dolomite and anhydrite. Earth Planet. Sci. Lett. 369, 220–232.
Scuderi, M.M., Collettini, C., Viti, C., Tinti, E., Marone, C., 2017. Evolution of shear fabric in granular fault gouge from stable sliding to stick slip and implications for fault slip mode. Geology 45 (8), 731–734.
Scuderi, M.M., Tinti, E., Cocco, M., Collettini, C., 2020. The role of shear fabric in controlling breakdown processes during laboratory slow-slip events. J. Geophys. Res., Solid Earth 125 (11), e2020JB020405.
Sibson, R., 1977. Fault rocks and fault mechanisms. J. Geol. Soc. (Lond.) 133, 191–213. https://doi.org/10.1144/gsjgs.133.3.0191.
Sibson, R.H., 1989. Earthquake faulting as a structural process. J. Struct. Geol. 11 (1–2), 1–14.
Smith, S.A.F., Holdsworth, R.E., Collettini, C., 2011. Interactions between low-angle normal faults and plutonism in the upper crust: insights from the Island of Elba, Italy. Bulletin 123 (1–2), 329–346.
Tan, Y.J., Waldhauser, F., Ellsworth, W.L., Zhang, M., Zhu, W., Michele, M., Chiaraluce, C., Beroza, C.G., Segou, M., 2021. Machine-learning-based high-resolution earthquake catalog reveals how complex fault structures were activated during the 2016–2017 central Italy sequence. Seismic Rec. 1 (1), 11–19.
Tembe, S., Lockner, D.A., Wong, T.F., 2010. Effect of clay content and mineralogy on frictional sliding behavior of simulated gouges: binary and ternary mixtures of quartz, illite, and montmorillonite. J. Geophys. Res., Solid Earth 115 (B3).
Tesei, T., Collettini, C., Carpenter, B.M., Viti, C., Marone, C., 2012. Frictional strength and healing behavior of phyllosilicate-rich faults. J. Geophys. Res., Solid Earth 117 (B9).
Tesei, T., Collettini, C., Barchi, M.R., Carpenter, B.M., Di Stefano, G., 2014. Heterogeneous strength and fault zone complexity of carbonate-bearing thrusts with possible implications for seismicity. Earth Planet. Sci. Lett. 408, 307–318. https://doi.org/10.1016/j.epsl.2014.10.021.
Tongiorgi, M., Rau, A., Martini, I.P., 1977. Sedimentology of early-alpine, fluviomarine, clastic deposits (Verrucano, Triassic) in the Monti Pisani (Italy). Sediment. Geol. 17 (3–4), 311–332.
Trippetta, F., Collettini, C., Meredith, P.G., Vinciguerra, S., 2013. Evolution of the elastic moduli of seismogenic Triassic Evaporites subjected to cyclic stressing. Tectonophysics 592, 67–79.
Verrucchi, C., Pandeli, E., Minissale, A., Andreotti, P., Paolieri, M., 1994. New data for the geochemical characterization of the Tuscan Paleozoic sequences (Northern Apennines, Italy). Mem. Soc. Geol. Ital. 48, 655–666.
Waldhauser, F., Ellsworth, W.L., Schaff, D.P., Cole, A., 2004. Streaks, multiplets, and holes: high-resolution spatio-temporal behavior of Parkfield seismicity. Geophys. Res. Lett. 31 (18).
Waldhauser, F., Michele, M., Chiaraluce, L., Di Stefano, R., Schaff, D.P., 2021. Fault planes, fault zone structure and detachment fragmentation resolved with high-precision aftershock locations of the 2016–2017 central Italy sequence. Geophys. Res. Lett. 48 (16), e2021GL092918.
Wallis, D., Lloyd, G.E., Phillips, R.J., Parsons, A.J., Walshaw, R.D., 2015. Low effective fault strength due to frictional-viscous flow in phyllonites, Karakoram Fault Zone, NW India. J. Struct. Geol. 77, 45–61.